

Physical model of back line-contact front-junction solar cells

Andres Cuevas

Citation: *J. Appl. Phys.* **113**, 164502 (2013); doi: 10.1063/1.4800840

View online: <http://dx.doi.org/10.1063/1.4800840>

View Table of Contents: <http://jap.aip.org/resource/1/JAPIAU/v113/i16>

Published by the [American Institute of Physics](#).

Additional information on J. Appl. Phys.

Journal Homepage: <http://jap.aip.org/>

Journal Information: http://jap.aip.org/about/about_the_journal

Top downloads: http://jap.aip.org/features/most_downloaded

Information for Authors: <http://jap.aip.org/authors>

ADVERTISEMENT

The advertisement banner for AIP Advances features a green and yellow background with abstract, flowing, wavy lines. The AIP Advances logo is prominently displayed in the center, with 'AIP' in blue and 'Advances' in green. To the right of the logo is a circular seal that reads 'Now Indexed in Thomson Reuters Databases'. Below the logo, the text 'Explore AIP's open access journal:' is followed by a list of three bullet points: 'Rapid publication', 'Article-level metrics', and 'Post-publication rating and commenting'.

AIPAdvances

Now Indexed in
Thomson Reuters
Databases

Explore AIP's open access journal:

- Rapid publication
- Article-level metrics
- Post-publication rating and commenting

Physical model of back line-contact front-junction solar cells

Andres Cuevas^{a)}

Research School of Engineering, The Australian National University, Canberra ACT 0200, Australia

(Received 15 November 2012; accepted 25 March 2013; published online 25 April 2013)

The analysis of advanced front-junction solar cells where the metal contact to the base region is locally formed on the back surface in the shape of lines usually requires numerical simulations. Here, we describe an approach based on a geometric formulation of carrier crowding towards the localized contact, in conjunction with a partition of the device in two distinct regions. This permits a one dimensional analysis of carrier flow, both in the region immediately adjacent to the contact and in the peripheral region surrounding it. The resulting model is simple enough to provide insight into the physics of device operation and reasonably accurate in cases of practical interest. By applying it to different cases, we identify unexpected anomalies and explain them in terms of the peculiar interplay between carrier transport and recombination that takes place in this type of solar cell. © 2013 AIP Publishing LLC. [<http://dx.doi.org/10.1063/1.4800840>]

I. INTRODUCTION

The suppression of recombination losses and the enhancement of photon absorption are well known paths to improve the conversion efficiency of solar cells. Pursuing both, advanced silicon solar cells use a dielectric layer that passivates the rear surface and, together with an overlying metal layer, forms an optical mirror. Perforations in the dielectric allow the metal to contact the semiconductor, providing an exit path for the electric current generated in it. In the common industrial implementation of solar cells with Partial Rear Contacts (PRC),^{1–3} the base region is p -type, the front n^+ electron-collector region is made by thermal diffusion of phosphorus, and the localized metal contacts at the rear are in the shape of lines. To further decrease recombination at the interface between metal and semiconductor, a localized p^+ hole-collector region is sometimes implemented, either by alloying aluminium or by diffusing boron.

The design of a PRC device structure usually requires a two-dimensional analysis.⁴ Optimizing the separation and size of the rear metal contacts is necessary to avoid excessive dissipative losses due to lateral currents while suppressing recombination. A possible approach is to use one of the several approximate analytical models that have been published^{5–10} or the analytical model presented in the Appendix to this paper. Alternatively, numerical computation, implemented in computer programs such as Sentaurus Device,¹¹ PC2D,¹² CoBo,¹³ or Quokka,¹⁴ offer detailed 2D or 3D simulation capabilities. A deep understanding of the physics of PRC device operation is, nevertheless, highly desirable to assess the impact that different material and device parameters may have on its potential to reach high conversion efficiencies.

Here, we describe a model that is sufficiently accurate to describe device operation in many cases of practical interest and simple enough to reveal the physics. Based on a

geometric approach proposed in Ref. 6, we follow an iterative method to determine the complete current-voltage characteristics of the device, including not only the open-circuit voltage but also the short-circuit current and the maximum output power. In prior work, we have shown that the model is in good agreement with Sentaurus Device for the case of circular contacts and low-injection conditions.¹⁵ Additional comparison and agreement, extended to high injection conditions and linear contacts is presented here. The purpose of this paper is to give a full description of the geometric model, clarifying not just its advantages but also its limitations. We then apply it to explore a wide range of dimensional and surface recombination parameters in order to evaluate their impact on solar cell performance. In the process, we have identified several interesting peculiarities in the operation of PRC solar cells, whose underlying physical causes can be understood with the help of the model.

II. GEOMETRIC MODEL

A. Regional approach

An intuitive way to conceive the PRC solar cell is as two sub-cells connected in parallel, as depicted in Fig. 1. The near-contact region is the most important of the two, since it is there that the metal contacts are formed and an electric current produced. The peripheral or lateral region has the function of harvesting photons and transferring the electrons and holes generated by them to the near-contact region. Holes can only travel across the lateral region via the p -type base. Fig. 1 qualitatively indicates that, as they eventually approach the rear metal contact, nearly all the holes (more accurately, those that have survived recombination) need to “squeeze in” within a diminishing cross-sectional area. This is usually referred to as “current crowding” where the total current remains approximately constant, but the current *density* increases strongly. It is reasonable to assume that current crowding occurs within a radial distance from the contact equal to the maximum possible distance in the vertical direction, that is, equal to the wafer thickness. This

^{a)}Telephone: 612-6125-3702. Fax: 612-6125-0506. E-mail: andres.cuevas@anu.edu.au.

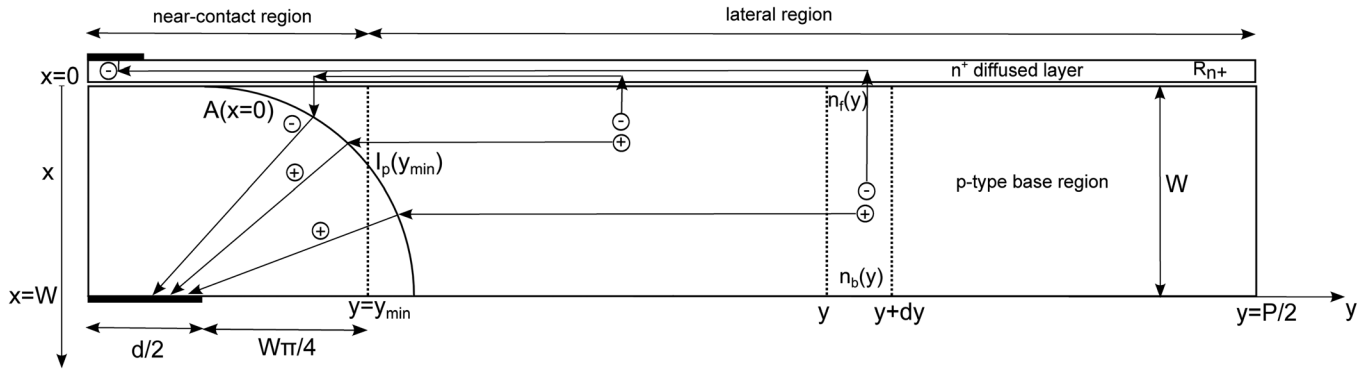


FIG. 1. Cross-section of a half-unit element of PRC solar cell. Drawn to scale for a wafer thickness $W = 150 \mu\text{m}$, rear contact dimension $d = 140 \mu\text{m}$, and pitch $P = 1666 \mu\text{m}$. The upper layer (not to scale) represents the n^+ diffusion. The diagram shows the near-contact and lateral regions in which the unit solar cell is divided for the analysis. Two possible paths of electrons and holes generated in the lateral region are qualitatively illustrated. In one possible path, the electrons exit the front contact; in the other the electrons recombine at the rear contact.

assumption is depicted in Fig. 1 as a circular arc of radius W centered on the edge of the metal contact stripe.

Turning now our attention to electrons, we can expect that, in well-designed devices operating at maximum power or short circuit conditions, most electrons will be able to reach the n^+ electron collector region placed at the front side of the solar cell and eventually exit via the front metal contact. Electrons generated in the peripheral region will flow laterally via the n^+ front diffusion, which offers a low resistance path. But some of those “peripheral” electrons, most in open-circuit conditions, will flow vertically down towards the rear contact to recombine there (see Fig. 1). They do so by crowding within a diminishing cross-sectional area, just like holes do. We will assume the same geometry, shown in Fig. 1, for minority carrier crowding as for majority carrier crowding. The reason for this is that, in the PRC device, the n^+ layer is never further away than a distance W . This means that the preferred path for electrons in the peripheral region will first go vertically to the n^+ electron collector layer and then laterally via the same n^+ layer, which possesses a high conductivity for electrons (see Fig. 1). Therefore, even if the minority carrier diffusion length in high quality silicon is usually much greater than the wafer thickness W , only those electrons generated within a distance W of the metal contact will follow a direct path towards it. We can therefore expect that the maximum extent of the “sphere of influence” of the rear contact in terms of minority carrier recombination will be approximately equal to the wafer thickness W in all directions.

Let us proceed to analyze the two regions in which we have divided the solar cell, starting with the peripheral one and concluding with the near-contact region. But first, we need to define a vertical boundary between the two in order to compute the number of photons absorbed in each of them. Examining the geometry of the crowding region, we can establish an approximate boundary as the average horizontal distance from points on the cylindrical surface of radius W to the center of the rear contact, that is, $y_{\min} = d/2 + W\pi/4$. We consider here PRC cells having linear contacts of width d separated a distance (or pitch) P . It is sufficient to model a unit solar cell containing just one rear contact and having a rectangular aperture area $A_0 = P \times 1 \text{ cm}$ defined by the pitch

P and a unit length of 1 cm. The rear metal contact fraction therefore is $f_c = d/P$. Due to symmetry, only half a unit cell needs to be analyzed, as shown in Fig. 1.

B. Analysis of the peripheral region

Let us consider the lateral region, comprised between a maximum y dimension defined by the aperture area of the half unit cell, $y_{\max} = P/2$ and a minimum dimension $y_{\min} = d/2 + W\pi/4$. The purpose of this section is to quantify the number of electrons and holes that, once generated in this region, flow into the near-contact region. The driving force for the electron and hole currents is a gradient of their respective electrochemical potentials; therefore, we can expect that the lateral transport of carriers will be at the expense of a certain reduction in the difference between those two potentials. In other words, the flow of the lateral currents will be accompanied by a voltage drop, a phenomenon frequently described as a series resistance effect. As we will see, such effect can be significant when the distance travelled by carriers is of the order of several millimetres. Needless to say, we will also need to account for recombination losses in the peripheral region. But, as a starting point, let us imagine for a moment that those losses are negligible. Electrons and holes are generated uniformly across the area of the solar cell. Each surface element of area $dy \times 1 \text{ cm}$ (see Fig. 1) will contribute to the hole current a quantity $J_{ph} \times dy \times 1 \text{ cm}$ (and an equal quantity to the electron current), where J_{ph} is the photogenerated current density. The lateral hole current $I_p(y)$, will increase from the farthest point on the right $y_{\max} = P/2$ towards the left, as more and more elements contribute to it. At a certain position y , its value will be

$$I_p(y)|_{no\ recomb} = J_{ph} \left(\frac{P}{2} - y \right) \cdot 1 \text{ cm}. \quad (1)$$

The hole current calculated at the boundary between the two regions $y = y_{\min}$ gives one half (remembering that Fig. 1 represents only half of a unit solar cell) of the net current that flows into the near-contact region. Therefore, if there were no recombination losses in the peripheral region, the net particle flux transferred from it to the near-contact region would, expressed as a current, take a maximum value

$I_{net(no\ recomb)} = J_{ph} \times A_{lat}$, where $A_{lat} = (P - 2y_{min}) \times 1\text{ cm}$ is the area of the lateral region.

More generally, I_{net} will be the net result of the balance between generation and recombination in the peripheral region. An elementary volume of width dy will contribute to the hole current I_p an amount that results from the local difference between generation and recombination

$$I_p(y) = I_p(y + dy) - [J_{ph} - J_{rec}(y)] dy \text{ 1 cm}, \quad (2)$$

where $J_{rec}(y)$ includes bulk and surface (front and rear) recombination within that element of volume at position y . Note that in the case we are studying, holes flow towards the left and I_p is negative, therefore, Eq. (2) indicates that the magnitude (absolute value) of I_p increases towards the rear contact region. Since the recombination rate is generally dependent on the excess minority carrier concentration, we will need to determine the latter as a function of the lateral position. We will use the letter n , instead of Δn , to refer to the excess electron concentration, using a subindex f or b to indicate its value at the front surface or at the back surface, respectively.

Recombination in the front n^+ diffusion can be expressed by means of a *recombination current pre-factor* J_{of} that encompasses losses in the volume of the diffusion and at its surface. The definition of this parameter is, precisely, that J_{of} multiplied by the normalized electron hole product, calculated at the front edge of the quasi-neutral p-type base, gives the global recombination loss occurring within the front surface region¹⁶

$$R_{front} = J_{of} \frac{(p_0 + n_f) n_f}{q n_i^2}, \quad (3)$$

where n_f is the excess electron concentration at the front end of the base region, q is the elementary charge, n_i is the intrinsic carrier concentration, and $p_0 \approx N_A$ is the equilibrium hole concentration, approximately equal to the concentration of acceptors in the p-type base region. Note that although the thickness of the n^+ diffusion has been exaggerated in Fig. 1, in the geometric model we regard it as what Brendel has called a “conductive boundary layer,”¹³ with a relatively high conductivity and an idealized zero thickness, so that light absorption and carrier collection in that layer does not need to be calculated.

A key simplification in our analysis of the lateral region is to assume that at a given position y the excess carrier density is approximately constant in the vertical dimension. This is appropriate in many cases of practical interest for high performance silicon PRC solar cells, where the minority carrier diffusion length is greater than the wafer thickness and the rear surface is well passivated. Even if solar photons are predominantly absorbed near the front surface of the silicon wafer, the steady-state concentration of electrons and holes tends to be quite uniform over the thickness of the wafer in such devices. Therefore, within the lateral region we assume that $n_{lat}(x, y) \approx n_f(y)$, which circumvents the need to perform an analysis of the minority carrier concentration in the vertical direction and simplifies the determination of $J_{rec}(y)$ enormously.

In high quality silicon solar cells, recombination in the space charge region of the pn junction is usually very small, and is neglected in our model. Bulk recombination can be characterized by means of the minority (electron) carrier lifetime τ_n , which we use here as an effective parameter that may represent both defect-assisted and intrinsic recombination. Since recombination mechanisms are in general injection dependent, the value of τ_n needs to be calculated for the local carrier density $n_f(y)$. In the peripheral region the rear surface is passivated by a dielectric material; the recombination per unit area at that surface can be represented via a parameter $J_{0b(pass)}$. Alternatively, it could be represented by means of an injection dependent effective surface recombination velocity $S_{b(pass)}$. Adding the surface and bulk contributions, we can express the recombination current term J_{rec} in Eq. (2) as

$$J_{rec} \approx (J_{0f} + J_{0b(pass)}) \frac{(p_0 + n_f) n_f}{n_i^2} + q \frac{n_f W}{\tau_n}. \quad (4)$$

By assuming that the minority carrier concentration is approximately constant in the vertical x dimension, we oversimplify the analysis of the peripheral region. This can be especially inaccurate in short-circuit conditions where $n_f(y) \approx 0$, which in our assumption also means that $n_b(y) \approx 0$, implying zero bulk and surface recombination losses. As a consequence, our analysis tends to over-estimate the short-circuit current. Nevertheless, even in short-circuit conditions, the carrier concentration far from the contacts in a PRC device is sometimes greater than zero, in which case our analysis can determine short-circuit current losses with reasonable accuracy, as we shall see in Sec. III.

Once we have settled the matter of carrier recombination in the peripheral region, we can proceed to describing carrier motion in it. In order for holes to flow laterally through a p-type semiconductor material with finite conductivity, a gradient in the quasi-Fermi energy for holes E_{Fp} along the lateral dimension y is required. The hole current $I_p(y)$ can be expressed as¹⁷

$$I_p(y) = \frac{\sigma_p A(y)}{q} \frac{dE_{Fp}}{dy}. \quad (5)$$

In Eq. (5), the cross-sectional area for majority carrier flow is constant, $A(y) = W \cdot 1\text{ cm}^2$ and σ_p is the hole conductivity

$$\sigma_p \approx q \mu_p (N_A + n_f(y)). \quad (6)$$

In writing Eq. (6), we have assumed that, as mentioned before, the excess carrier concentration within an elementary volume is approximately constant in the vertical direction, equal to its value at the front, $n_f(y)$. Note that holes flow towards the left of the y axis in the case analyzed here, that is, I_p is negative. This means that the derivative of E_{Fp} in Eq. (5) must also be negative. The electrochemical potential for holes $-E_{Fp}$ is higher (more negative) on the right end of the peripheral region than on the left end, and the difference between both indicates that the flow of holes occurs at the expense of a loss of energy. This is frequently described by

means of an equivalent series resistance effect; an approximate analytical expression for such series resistance is derived in the Appendix.

Similarly, electrons flow laterally via the n^+ region, which has a sheet resistance R_{n^+} , driven by a small gradient of the quasi-Fermi energy for electrons E_{Fn}

$$I_n(y) = \frac{1 \text{ cm } dE_{Fn}}{qR_{n^+} dy}. \quad (7)$$

To write Eq. (7), we have assumed that the metal contact to the n^+ front region is placed precisely on top of the local rear contact. This means that electrons flow laterally in the same direction as holes, albeit via the n^+ region, rather than the base (see Fig. 1). Since electrons are negatively charged, their flow towards the left means that I_n is positive, which requires a positive gradient of E_{Fn} . The electrochemical potential for electrons is lower on the left end of the lateral region than on the right end, and the difference between both represents an energy loss that can be interpreted as an additional series resistance effect.

To simplify the mathematical derivations, we can express in units of Volts the local difference between the quasi-Fermi energies for electrons and holes across the pn junction as $V(y)$

$$V(y) = \frac{E_{Fn} - E_{Fp}}{q}. \quad (8)$$

The difference between the quasi-Fermi energies as a function of the lateral position $V(y)$ can be obtained by integration of Eqs. (5) and (7), noting that the electron and hole currents flowing out of a given elementary volume dy are equal, but with opposite sign

$$V(y) = V(y + dy) + I_p \left(\frac{1}{\sigma_p W} + R_{n^+} \right) \frac{dy}{1 \text{ cm}}. \quad (9)$$

Since the hole current I_p is negative, $V(y)$ decreases from the right end of the lateral region towards the left, as a consequence of the resistive voltage drops in both semiconductor layers.

The next step in the analysis is to determine the minority carrier concentration as a function of the lateral distance $n_f(y)$ from the relationship that exists between the pn product and the difference between the quasi-Fermi energies for electrons and holes

$$n_f(y)(p_o + n_f(y)) = n_i^2 \exp\left(\frac{V(y)}{kT/q}\right), \quad (10)$$

where k is the Boltzmann constant and T is the temperature in degrees Kelvin. The above analysis is valid for low or high injection conditions. Since $V(y)$ increases with distance from the contact, so will the excess carrier concentration. This means that recombination losses will also be greater in distant points of the peripheral region than in points nearer the contact region, particularly surface recombination losses, which as Eq. (4) indicates, are proportional to the square of the excess carrier concentration.

Due to the fact that the excess carrier concentration $n_f(y)$ is not uniform in the lateral dimension, it is necessary to divide the peripheral region in multiple vertical slices (we have used 100 in this study) and solve the above equations sequentially for each of them. It is convenient to start the analysis from the farthest slice, assuming an initial value for the minority carrier concentration there $n_f(P/2)$. As Eq. (10) indicates, this is equivalent to assume an initial value for the voltage at that position, $V(P/2)$. Adjacent elementary slices are linked via Eqs. (2) and (9). Eventually, the net current injected from the peripheral region into the near-contact region I_{net} can be determined by subtracting from the total photogeneration occurring in the periphery the sum of all the contributions to recombination in it

$$I_{net} = \left(J_{ph} - \sum J_{rec} \right) A_{lat}, \quad (11)$$

where $A_{lat} = (P - 2y_{min}) \times 1 \text{ cm}$ is the area of the lateral region. Alternatively, I_{net} can also be calculated as the value of the hole current at the boundary between the lateral and near-contact regions $I_{net} = 2 \times |I_p(y_{min})|$, taking care of the fact that the half unit cell shown in Fig. 1 only gives half the net injected current.

To find a global solution for the complete device, it is necessary to follow an iterative procedure, changing the value of $n_f(P/2)$ until self-consistency is achieved. Such self-consistency needs to apply simultaneously to the peripheral and near-contact regions. In addition to I_{net} , a second link between the two regions is established by the value of the minority carrier concentration at the boundary between both $n_f(y_{min})$. The value of $n_f(y_{min})$ that results from the analysis of the peripheral region via Eq. (10) is used as an input for the analysis of the near-contact region, which is described in Sec. II C.

C. Analysis of the near-contact region

The trajectories of electrons that flow towards the rear contact to recombine there and the trajectories of holes as they flow towards the contact may be radial, as qualitatively indicated in Fig. 1. It would seem that a two-dimensional analysis of the region surrounding the rear contact is indispensable, but in this section we show that a one dimensional analysis can give an approximate solution to the problem.

To analyze the near-contact region, shown in Fig. 2, we divide it into multiple elements of distance dx in the vertical direction (200 have been used in this paper). Considering an elementary volume defined by a vertical distance dx , the continuity equation for the electron current density J_n takes into account possible photogeneration G_L and recombination R_v in that volume

$$-J_n(x + dx) = -J_n(x) + qG_L(x)dx - qR_v(x)dx. \quad (12)$$

To calculate the volume photogeneration rate as a function of position $G_L(x)$, we have used optical models similar to those described in Refs. 18 and 19, together with the AM1.5G solar spectrum and published data for the absorption coefficient of silicon.²⁰ Carrier recombination in the

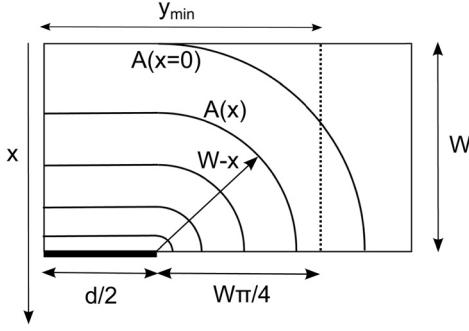


FIG. 2. Cross-sectional diagram of the near-contact region. Wafer thickness $W = 150 \mu\text{m}$ and contact dimension $d = 170 \mu\text{m}$. y_{\min} designates the average vertical boundary between the near-contact region and the peripheral region.

volume is calculated using injection dependent Shockley-Read-Hall statistics (set to zero in this study) and an empirical expression for Auger and band-to-band recombination.²¹

To analyze the first element, situated at $x=0$, we need to remember that the peripheral region injects into the near-contact region an equal number of electrons and holes. This influx of electron-hole pairs can be considered in the analysis of the near-contact region by means of an effective photogeneration term. By assuming that this effective photogeneration occurs as a delta function at $x=0$, we ensure that in short-circuit conditions all the electrons supplied by the peripheral region remain “collected,” since they are all deemed to be generated right at the front electron-collecting contact. The effective generation term contributed by the lateral region, expressed as a current density per unit area, is $J_{\text{net}} = I_{\text{net}}/A_{\text{NC}}$, where $A_{\text{NC}} = 2y_{\min} \times 1 \text{ cm}$ is the aperture area of the near-contact region.

The continuity of the excess minority carrier concentration between the peripheral region $n_f(y_{\min})$ and the near-contact region $n_f(x=0)$ permits us to calculate the recombination losses at the front surface of the near-contact region, that is at $x=0$, using the boundary condition (3). It is reasonable to assume that n_f is constant over the whole front surface area of the near-contact region, $n_f(x=0) = n_f(y_{\min})$.

Proceeding next to studying carrier transport, we note that when a net current density J flows through the device, at any point x it is composed of the sum of the electron and hole current densities, that is,

$$J_n(x) = J - J_p(x). \quad (13)$$

In general, the electron and hole currents are made up of a diffusion term and a drift term, but both can be lumped together by defining an effective diffusion coefficient D_{eff} ,²²

$$D_{\text{eff}} = \frac{(n+p)D_n D_p}{nD_n + pD_p}, \quad (14)$$

where D_n and D_p are the diffusion coefficients for electrons and holes. At this point, we need to incorporate into the analysis the current-crowding effects mentioned in Sec. II A. As they flow towards the rear contact, holes and electrons traverse a diminishing cross-sectional area. By examining the geometry in Fig. 2, this cross-sectional area can be expressed as a function of the vertical position x as

$$A(x) = 1 \text{ cm} [d + \pi(W-x)], \quad (15)$$

where 1 cm is the assumed length of the linear contacts and d is their width. In cases where the pitch may be very small, the radius of the outer surface that defines the extent of the crowding region needs to be capped so that the area of such outer surface is smaller or equal to the area of the unit solar cell, that is, $A(x=0) \leq A_0$. A graphical explanation of this condition can be found in Ref. 6.

After some algebra, the electron current density, defined as the total electron current divided by the aperture area of the unit solar cell, $J_n = I_n/A_0$, can be expressed as

$$J_n(x) = q \frac{A(x)}{A_0} D_{\text{eff}} \frac{dn}{dx} + J \frac{nD_n}{nD_n + pD_p}. \quad (16)$$

The next step is to integrate Eq. (16) over a small interval dx within which the electron current can be considered approximately constant

$$n(x+dx) = n(x) + \frac{J_n(x)A_0}{qA(x)D_{\text{eff}}} dx - \frac{JA_0}{qA(x)D_{\text{eff}}} \frac{nD_n}{nD_n + pD_p} dx. \quad (17)$$

In deriving Eqs. (16) and (17), which are valid for any injection level, the only assumptions have been that the excess concentrations of both carriers are approximately equal and that $dn/dx = dp/dx$. From Eq. (17), we can now determine the value of the minority carrier concentration at the back n_b , and apply the corresponding boundary condition. The recombination per unit area at the rear metal contact, including the p^+ region sometimes present underneath it, can be represented via a recombination current pre-factor $J_{0\text{cont}}$

$$R_{\text{cont}} = J_{0\text{cont}} \frac{f_c}{f_{\text{NC}}} \frac{(p_0 + n_b) n_b}{qn_i^2}. \quad (18)$$

Note that we have taken into account the fact that the contact only covers a fraction of the rear surface. Since we are now analyzing the near-contact region, such fraction is f_c/f_{NC} , where $f_{\text{NC}} = 2y_{\min}/P$ is the portion of the elementary solar cell occupied by the near-contact region (see Fig. 1).

In low-injection conditions, recombination at the back surface can alternatively be expressed by means of an effective surface recombination velocity. An expression for the carrier concentration at the back contact, n_b , may be found by stating that the rate at which carriers flow towards the surface must be equal to the rate at which they recombine there

$$n_b = \frac{J_n(W)}{q(f_c/f_{\text{NC}})S_{\text{cont}}}, \quad (19)$$

where $J_n(W)$ is the electron current reaching the contact, and S_{cont} is the effective surface recombination velocity of the contact, including a possible p^+ region. Nevertheless, in high and intermediate injection conditions, the boundary condition (18) is more robust and has been adopted in our model.

In the passivated parts of the rear surface of the near-contact region, the minority carrier concentration varies along the y direction from a relatively low $n_{b(cont)}$ to a comparatively high $n_{b(pass)}(y=W) \approx n_f$, making an accurate determination of surface recombination complex. In the calculations shown in Sec. III, we have set to zero the parameter that characterizes the passivated surface, that is, $J_{0b(pass)} = 0$.

Expressions (16) and (17) show that, in a PRC solar cell, the constriction of minority carrier flow within a small cross-sectional area is equivalent to reducing the minority carrier diffusion coefficient. The cross sectional area $A(x)$ is much smaller near the back contact than at the front. This has the consequence of hindering the diffusion of minority carriers towards the contact, thus reducing the rate at which they may recombine there.

D. Device voltage

The terminal voltage of an n^+pp^+ solar cell is given by the difference between the electron Fermi energy, E_{Fn} , determined at the metal-contacted n^+ region, and the hole Fermi energy, E_{Fp} , determined at the metal-contacted p^+ (or p) region. This electrochemical potential difference can be broken down in three parts. One is the shift of the electron Fermi energy, E_{Fn} , with respect to its equilibrium position, E_F , which is given by the ratio of the total electron concentration at the front to its equilibrium value. The second component is the shift of the hole Fermi energy, E_{Fp} , with respect to its equilibrium position, E_F , which is given by the ratio of the total hole concentration at the back to its equilibrium value.

The voltage of the solar cell can, therefore, be determined once the excess carrier concentrations at the front n_f and back n_b of the base region are known

$$V = \frac{kT}{q} \ln \left(\frac{(n_o + n_f)(p_o + n_b)}{n_i^2} \right) + V_{Base}. \quad (20)$$

The third term in this expression, V_{Base} , accounts for a possible electrostatic potential drop across the base region that can result from electric fields within it. As a consequence of the different mobilities of electrons and holes, an electric field may develop within the wafer to assist the motion of holes and help maintain charge neutrality. The resulting *Demmer effect* voltage can be significant in lowly doped silicon when the carrier profile is highly non-uniform. In addition, the flow of a current density J through the semiconductor region, is accompanied by an Ohmic electrostatic potential drop. Both terms are included in the following expression for the electric field, whose integration gives V_{Base}

$$\xi = \frac{kT}{q} \frac{\mu_p - \mu_n}{n\mu_n + p\mu_p} \frac{dn}{dx} + \frac{JA_0}{qA(x)(n\mu_n + p\mu_p)}. \quad (21)$$

Note that the Ohmic term in Eq. (21) includes the cross sectional area $A(x)$ in the denominator to account for current crowding towards the localized rear contact. This term, or its equivalent manifestation as a series resistance, can be quite significant in PRC solar cells.

A complete I-V characteristic curve can be determined point by point by iterating $n_f(P/2)$ until the carrier density profiles in both the lateral and vertical directions are consistent with the corresponding output current and the surface boundary conditions. To perform the calculations shown in the Sec. III, the iterative process was implemented in Microsoft Excel, extending a pre-existing 1D model.^{22,23}

III. EXAMPLES OF APPLICATION

As a representative example of a partial rear contact cell structure, we study the case of a p-type wafer with a thickness $W = 150 \mu\text{m}$, and $d = 150 \mu\text{m}$ wide linear metal contacts on the rear surface. This means that the extension of the near-contact region is relatively small, $2y_{min} = 0.0386 \text{ cm}$, compared to the range of pitch values explored in the calculations. To start with, we assume a typical value for the dopant density of $N_A = 1 \times 10^{16} \text{ cm}^{-3}$, which for that wafer thickness, implies a sheet resistance of the wafer of $97 \Omega/\text{sq}$. We will assume that the front diffused region presents a sheet resistance of $50 \Omega/\text{sq}$, which also contributes to the lateral voltage drop due to the flow of electrons through it, as described by Eq. (7). Nevertheless, the presence of a metal grid on the front surface region means that its effective sheet resistance will generally be lower. The simulations presented below are not very sensitive to this parameter, as long as it is within reasonably low values.

For the recombination current pre-factor that characterizes the front surface region, we use $J_{0f} = 100 \text{ fA}\cdot\text{cm}^{-2} = 10^{-13} \text{ A}\cdot\text{cm}^{-2}$ as representative of industrial best practice. In the results presented below, we have only included intrinsic (Auger and band to band) injection and dopant dependent bulk recombination and set to zero the recombination at the passivated areas of the rear surface. The temperature is 300 K. The photogeneration corresponds to that produced by the AM1.5G spectrum, together with front surface texturing and a good back surface mirror, which usually accompanies the localized formation of metal contacts. This leads to a cumulative photogeneration at one sun of $N_{ph(total)} = 2.5 \times 10^{17} \text{ cm}^{-2}$, or $J_{ph} = 40.02 \text{ mA}\cdot\text{cm}^{-2}$. In the metal-contacted areas the actual photogeneration will be slightly lower, due to a lower back reflectivity, but given that they occupy only a small fraction of the device, neglecting this difference does not produce large errors. The calculations in this paper do not include shading or resistive losses neither due to a front metal grid nor any contact resistance between metal and semiconductor. These additional contributions can easily be added to the model.

A. Influence of contact recombination

Let us commence by studying the impact of contact recombination on device performance, varying the recombination current pre-factor that characterizes it between $J_{0cont} = 5 \times 10^{-9} \text{ A}\cdot\text{cm}^{-2}$ and $J_{0cont} = 1 \times 10^{-13} \text{ A}\cdot\text{cm}^{-2}$. In the case of a silicon wafer doped with $N_A = 10^{16} \text{ cm}^{-3}$, these pre-factors correspond to low-injection surface recombination velocities of $S_{cont} = 3.32 \times 10^6 \text{ cm s}^{-1}$ (kinetic limit in silicon) and $S_{cont} = 66.4 \text{ cm s}^{-1}$, respectively. A low contact

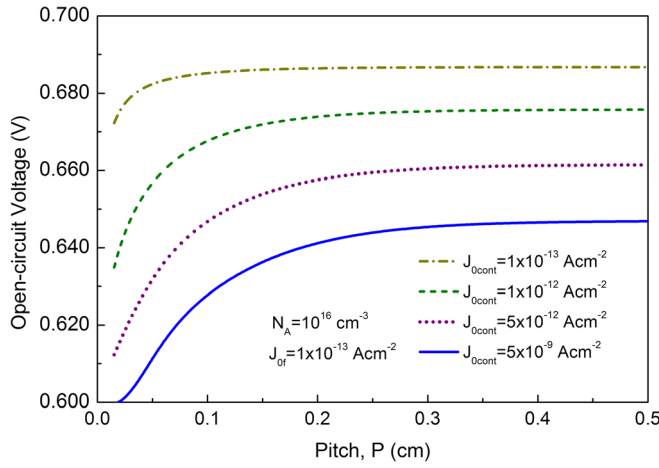


FIG. 3. Open-circuit voltage as a function of the pitch for $N_A = 10^{16} \text{ cm}^{-3}$, $d = 150 \mu\text{m}$, $W = 150 \mu\text{m}$, and $J_{0f} = 10^{-13} \text{ A cm}^{-2}$. Contact recombination ranging from $J_{0cont} = 5 \times 10^{-9} \text{ A cm}^{-2}$ to $J_{0cont} = 1 \times 10^{-13} \text{ A cm}^{-2}$.

recombination can be achieved, for example, by inserting a p^+ region beneath the metal-semiconductor contact.

Contact recombination has a large influence on the open-circuit voltage V_{oc} , as can be seen in Fig. 3, where it is plotted as a function of the pitch for different J_{0cont} between 5 nA cm^{-2} and 100 fA cm^{-2} . V_{oc} increases with the pitch, as the fraction of metal-contacted area decreases. The short-circuit current density, J_{sc} , shown in Fig. 4, also increases with the pitch. A high contact recombination gives a lower J_{sc} , especially at low pitch values, as the fraction of rear surface with poor or no passivation increases. The fill factor FF (Fig. 5) degrades slightly faster with the pitch for low contact recombination than for high J_{0cont} . The combination of the above three parameters results in a maximum of the conversion efficiency that, as shown in Fig. 6, shifts to lower pitch values as contact recombination decreases. Since the maximum occurs near $P = 0$ when $J_{0cont} = 100 \text{ fA cm}^{-2}$, it is clear that in that case recombination at the metal-contacted rear surface is no longer the dominant mechanism and the benefit of restricting the rear

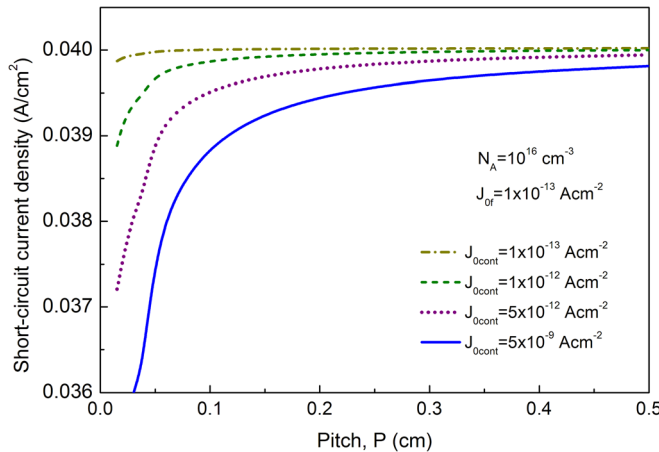


FIG. 4. Short-circuit current density as a function of the pitch for $N_A = 10^{16} \text{ cm}^{-3}$, $d = 150 \mu\text{m}$, $W = 150 \mu\text{m}$, and $J_{0f} = 10^{-13} \text{ A cm}^{-2}$. Contact recombination ranging from $J_{0cont} = 5 \times 10^{-9} \text{ A cm}^{-2}$ to $J_{0cont} = 1 \times 10^{-13} \text{ A cm}^{-2}$.

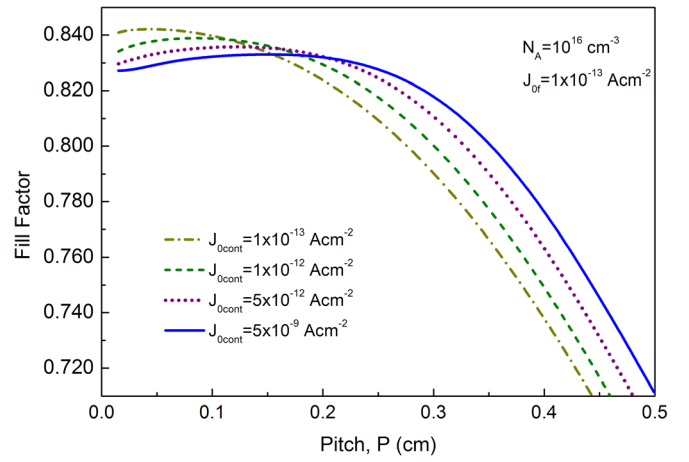


FIG. 5. Fill factor as a function of the pitch for $N_A = 10^{16} \text{ cm}^{-3}$, $d = 150 \mu\text{m}$, $W = 150 \mu\text{m}$, and $J_{0f} = 10^{-13} \text{ A cm}^{-2}$. Contact recombination ranging from $J_{0cont} = 5 \times 10^{-9} \text{ A cm}^{-2}$ to $J_{0cont} = 1 \times 10^{-13} \text{ A cm}^{-2}$.

contact to lines is very small. In fact, for such low recombination rate at the contact, V_{oc} saturates at a value just 2 mV below the limit of 689 mV imposed by recombination at the front n^+ region plus Auger recombination in the bulk.

B. Discussion of the physics

Observing the behavior of the open-circuit voltage V_{oc} in Fig. 3, one could find surprising that V_{oc} saturates at a different value depending on the level of passivation of the contact, despite the fact that the latter represents a vanishing fraction of the total cell area. Indeed, analytical models for V_{oc} , such as that described in the Appendix, predict that for very large pitch values V_{oc} should converge towards the same limit for all the cases of contact recombination. Clearly, as indicated by the results in Fig. 3, which we have confirmed by independent numerical simulations,²⁴ that is not the case. To understand why, we have plotted in Fig. 7 the net current I_{net} injected by the lateral region into the near-contact one, taking as an example the case of

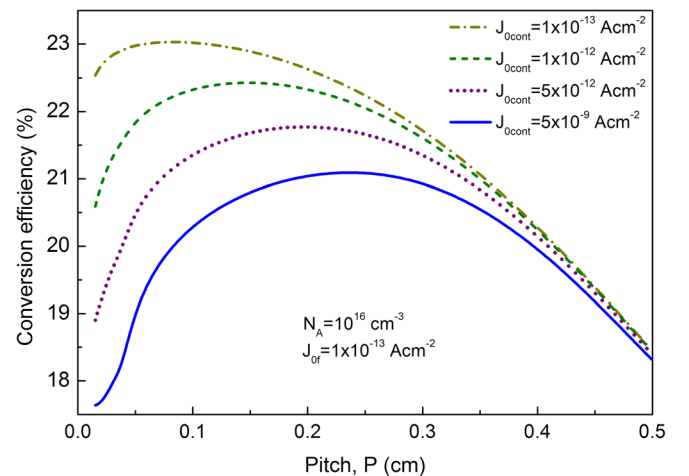


FIG. 6. Conversion efficiency as a function of the pitch for $N_A = 10^{16} \text{ cm}^{-3}$, $d = 150 \mu\text{m}$, $W = 150 \mu\text{m}$, and $J_{0f} = 10^{-13} \text{ A cm}^{-2}$. Contact recombination ranging from $J_{0cont} = 5 \times 10^{-9} \text{ A cm}^{-2}$ to $J_{0cont} = 1 \times 10^{-13} \text{ A cm}^{-2}$.

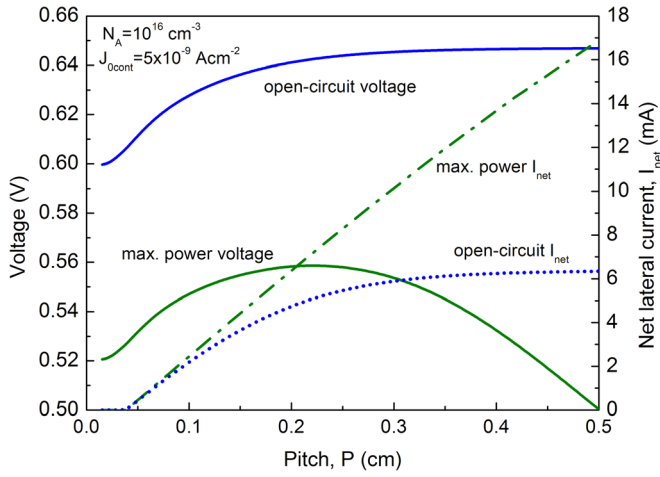


FIG. 7. Open-circuit and maximum power voltage as a function of the pitch for $N_A = 10^{16} \text{ cm}^{-3}$, $d = 150 \mu\text{m}$, $W = 150 \mu\text{m}$, $J_{0f} = 10^{-13} \text{ A cm}^{-2}$, and $J_{0cont} = 5 \times 10^{-9} \text{ A cm}^{-2}$. The net current injected from the peripheral region to the near-contact region is given for both open-circuit and maximum power conditions.

$J_{0cont} = 5 \text{ nA/cm}^2$. It can be observed that in open-circuit I_{net} saturates at approximately the same pitch as V_{oc} . For a pitch $P = 0.4 \text{ cm}$, the lateral region represents 90% of the total area of the unit cell, and the current photogenerated is 14.5 mA . But as Fig. 7 indicates, only $I_{net} = 6.3 \text{ mA}$ are injected to the near-contact region, the rest having recombined in the peripheral region. The injection of this I_{net} has the same effect as if the near-contact region was working under illumination concentrated five times, which helps to increase V_{oc} by approximately 43 mV .

The reason for the recombination loss that causes I_{net} to saturate can be understood by looking at the excess minority carrier concentration as a function of the lateral position y , which is plotted in Fig. 8 for $P = 0.4 \text{ cm}$. It can be noticed that the carrier concentration increases markedly with the

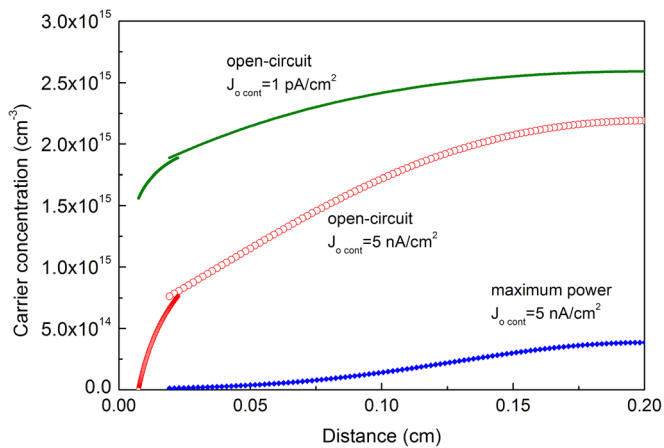


FIG. 8. Minority carrier concentration as a function of the lateral distance from the center of the unit solar cell for a half-pitch value of 0.2 cm in open-circuit and maximum power conditions. Two cases of contact recombination are shown for open-circuit conditions, $J_{0cont} = 5 \times 10^{-9} \text{ A cm}^{-2}$ and $J_{0cont} = 1 \times 10^{-12} \text{ A cm}^{-2}$. Other parameters are $N_A = 10^{16} \text{ cm}^{-3}$, $d = 150 \mu\text{m}$, $W = 150 \mu\text{m}$, and $J_{0f} = 10^{-13} \text{ A cm}^{-2}$. The boundary between the lateral and near-contact regions is marked by a discontinuity in the curves.

distance into the peripheral region and is well above the value of $n_f = 7.4 \times 10^{14} \text{ cm}^{-3}$ at the front of the near-contact region that is behind the $V_{oc} = 647 \text{ mV}$ achieved in this case. As discussed in Sec. II B, this increase in carrier concentration is associated to the gradient in the electrochemical potential needed to sustain the flow of current along the lateral dimension. In fact, the local pn junction voltage at the extreme point is $V(P/2) = 685 \text{ mV}$.

Losses in the peripheral region are mostly due, in the example we are discussing, to recombination at the front n^+ collector. Since these losses are quadratically proportional to n_f , it is essential to reduce n_f to increase the net current that can be contributed by the lateral region. This is precisely what happens at the maximum power point. The device voltage is then $V_{mp} = 534 \text{ mV}$, low enough to make the carrier concentration in the peripheral region also low, thus averting most recombination losses. As can be seen in Fig. 8, in maximum power conditions, the carrier density also tends to increase with distance, which produces some recombination, but small enough to permit an approximately linear increase of the net current contributed by the peripheral region I_{net} as its size increases, as shown in Fig. 7. For $P = 0.4 \text{ cm}$, $I_{net} = 13.7 \text{ mA}$, which means that only 5% of carriers generated in the peripheral region recombine there. This I_{net} can be expressed as a current density of 34.2 mA/cm^2 , which represents 91% of the output current density $J_{mp} = 37.5 \text{ mA/cm}^2$. It is worth noting that the electrons constituting this I_{net} flow directly out of the front metal contact and do not contribute to increasing the voltage measured between the terminals of the near-contact region, as they do in open-circuit. Nevertheless, the holes that also constitute I_{net} do flow down the vertical dimension of the near-contact crowding region, resulting in a voltage drop of about 10 mV in this case. In addition to this voltage loss due to crowding in the near-contact region, the flow of holes as majority carriers in the peripheral region occurs at the cost of an additional voltage drop across the length of that region of 89 mV . The sum of both voltage drops may be represented by an effective series resistance of $2.73 \Omega \text{ cm}^2$, which plays a major part in the relatively low $FF = 0.779$ determined for this particular solar cell. To control such resistive losses it is necessary to reduce the pitch. Fig. 7 indicates that the maximum power voltage reaches a broad maximum for $P = 0.2 \text{ cm}$. In that case, the lateral voltage drop is just 19 mV and that due to crowding in the near-contact region is 5 mV . The result is a lower series resistance of $0.66 \Omega \text{ cm}^2$, a higher $V_{mp} = 559 \text{ mV}$ and $FF = 0.832$.

The analysis of maximum power conditions for the case of a well passivated contact, $J_{0cont} = 1 \text{ pA/cm}^2$, reveals similar physics. The need to suppress an excessive build-up of carriers in the peripheral region leads to a relatively low $V_{mp} = 539 \text{ mV}$ for $P = 0.4 \text{ cm}$, just 4 mV higher than in the previous case. It is clear that the optimum terminal voltage is mostly determined by the need to maximize the contribution of the large-area peripheral region to the output current. Indeed, although not plotted in Fig. 7, the dependence of I_{net} on the pitch is practically the same as in the previous case, with the result of $J_{mp} = 37.6 \text{ mA/cm}^2$, again similar to the previous case. This explains why the conversion efficiency is

practically independent of contact recombination at large pitch values, as shown in Fig. 6.

Things are different in open-circuit conditions, where a low contact recombination $J_{0cont} = 1 \text{ pA/cm}^2$ permits that the carrier concentration at the contact to be considerably higher, $n_{cont} = 1.56 \times 10^{15} \text{ cm}^{-3}$. The carrier concentration increases further within the near-contact region to reach $n_f = 1.9 \times 10^{15} \text{ cm}^{-3}$ at the front. As can be observed in Fig. 8, n_f remains very high over the whole distance of the peripheral region, leading to a high recombination loss and leaving very few net carriers available for lateral transfer, resulting in a low injected current of just $I_{net} = 2.3 \text{ mA}$. This is no obstacle to achieving a high open-circuit voltage $V_{oc} = 676 \text{ mV}$.

In contrast, for the case of a very high surface recombination velocity at the contact $J_{0cont} = 5 \text{ nA/cm}^2$, the minority carrier concentration at the back contact is very low, $n_{cont} < 10^{12} \text{ cm}^{-3}$. This makes it very difficult to build-up the carrier concentration in the vertical direction of the near-contact region, despite a higher lateral injection of carriers. As mentioned above, such lateral injection saturates at high pitch values, and as a result V_{oc} saturates at a lower value for the case of a high contact recombination than for the case of a low contact recombination. Interestingly, given that the maximum power is approximately the same in both cases, the difference in V_{oc} produces a reversal in the trend of the respective fill factor values for large pitch, as was noted in the description of Fig. 5.

C. Influence of wafer doping

To explore the range of applicability of the geometric model to high injection conditions, let us reduce the wafer doping by a factor of ten, that is, to $N_A = 10^{15} \text{ cm}^{-3}$, corresponding to a resistivity of $13.5 \Omega\text{-cm}$. We consider the case of a reasonably low contact recombination, characterized by means of a recombination current pre-factor $J_{0cont} = 10^{-12} \text{ A}\cdot\text{cm}^{-2} = 1 \text{ pA/cm}^2$. The recombination current pre-factor that characterizes the front surface region is $J_{0f} = 100 \text{ fA}\cdot\text{cm}^{-2}$, the same as in the previous example. To assess the applicability of the model, we have performed simulations

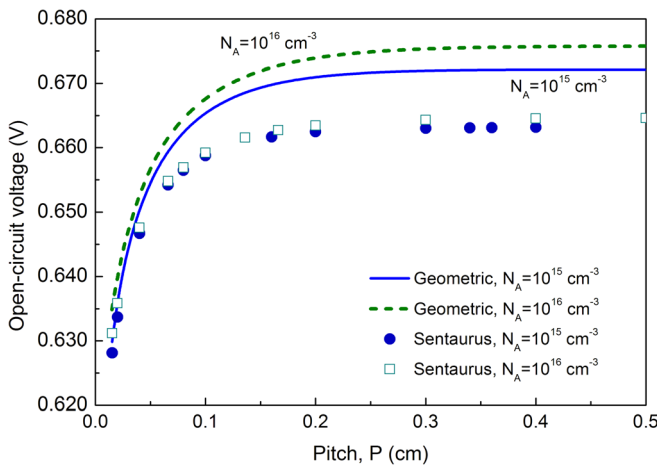


FIG. 9. Open circuit voltage as a function of the pitch for two different wafer dopant concentrations $N_A = 10^{15} \text{ cm}^{-3}$ and $N_A = 10^{16} \text{ cm}^{-3}$. The front and back surface recombination factors are $J_{0f} = 100 \text{ fA}\cdot\text{cm}^{-2}$ and $J_{0cont} = 1000 \text{ fA}\cdot\text{cm}^{-2}$. Other parameters are $d = 150 \mu\text{m}$, $W = 150 \mu\text{m}$.

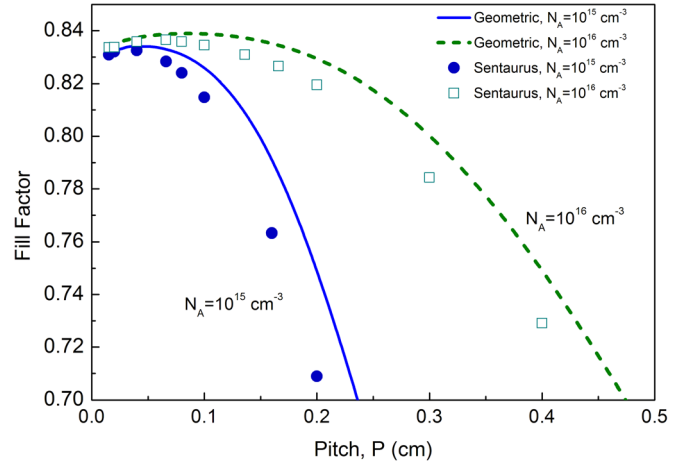


FIG. 10. Fill factor as a function of the pitch for two different wafer dopant concentrations $N_A = 10^{15} \text{ cm}^{-3}$ and $N_A = 10^{16} \text{ cm}^{-3}$. The front and back surface recombination factors are $J_{0f} = 100 \text{ fA}\cdot\text{cm}^{-2}$ and $J_{0cont} = 1000 \text{ fA}\cdot\text{cm}^{-2}$. Other parameters are $d = 150 \mu\text{m}$, $W = 150 \mu\text{m}$.

with Sentaurus Device. The main electrical parameters of the solar cell, J_{sc} , V_{oc} , FF , and efficiency are shown in Figs. 9–12, comparing the high-injection case of $N_A = 10^{15} \text{ cm}^{-3}$ to the low-injection case of $N_A = 10^{16} \text{ cm}^{-3}$. In general, a good agreement between the geometric model and Sentaurus simulations can be observed.

The open-circuit voltage V_{oc} does not change much with wafer doping for the case of $J_{0cont} = 1 \text{ pA/cm}^2$. The relatively large discrepancy between the values calculated with the geometric model and with Sentaurus (Fig. 9) is partly attributable to the inclusion of band gap narrowing in the latter, which increases the effective intrinsic carrier density, and to different models for Auger recombination. The main effect of reducing the wafer doping is that the FF (Fig. 10) and the efficiency (Fig. 11) peak at a much lower pitch and degrade faster as the pitch increases beyond the optimum. The reduction in maximum achievable efficiency due to the reduced dopant density is, however, quite small.

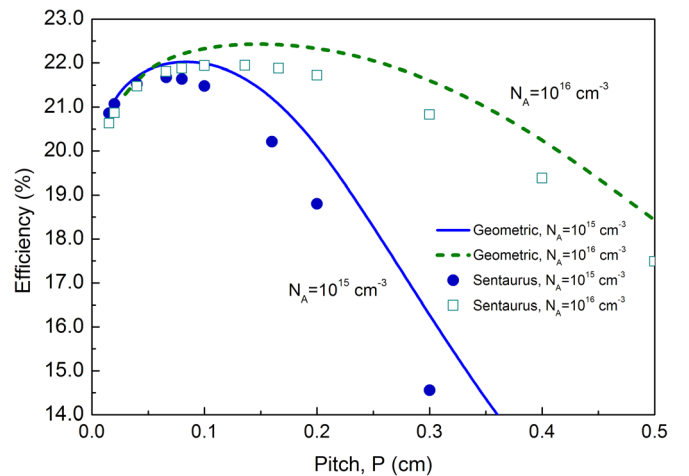


FIG. 11. Conversion efficiency as a function of the pitch for two different wafer dopant concentrations $N_A = 10^{15} \text{ cm}^{-3}$ and $N_A = 10^{16} \text{ cm}^{-3}$. The front and back surface recombination factors are $J_{0f} = 100 \text{ fA}\cdot\text{cm}^{-2}$ and $J_{0cont} = 1000 \text{ fA}\cdot\text{cm}^{-2}$. Other parameters are $d = 150 \text{ mm}$, $W = 150 \text{ mm}$.

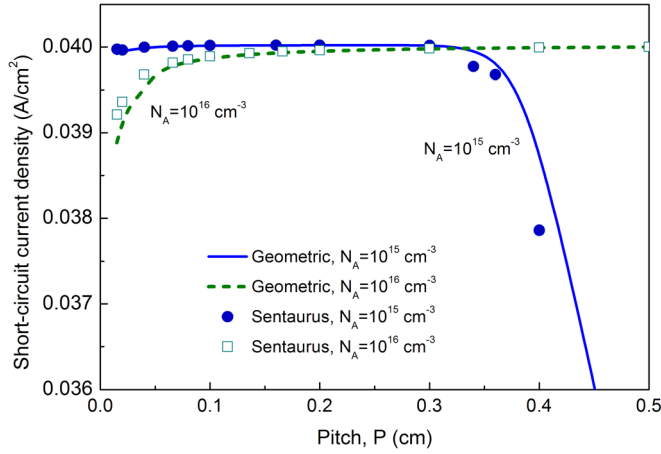


FIG. 12. Short circuit current as a function of the pitch for two different wafer dopant concentrations $N_A = 10^{15} \text{ cm}^{-3}$ and $N_A = 10^{16} \text{ cm}^{-3}$. The front and back surface recombination factors are $J_{0f} = 100 \text{ fA cm}^{-2}$ and $J_{0cont} = 1000 \text{ fA cm}^{-2}$. Other parameters are $d = 150 \text{ mm}$, $W = 150 \text{ mm}$.

An interesting feature can be observed in the dependence of the short-circuit current density J_{sc} with the pitch (Fig. 12). For $N_A = 10^{15} \text{ cm}^{-3}$, J_{sc} drops rapidly for pitch values larger than 0.35 cm. To understand this unexpected behaviour, confirmed by Sentauros simulations, we have plotted in Fig. 13 the carrier concentration profile in the lateral region for $P = 0.4 \text{ cm}$. We can see that, even if short-circuit conditions exist in the near-contact region, as shown by $n_f(y_{min}) = 0$, the pn junction is in forward bias in the peripheral region far from the contact. Many carriers generated there recombine *in-situ*, mostly at the front n^+ electron collector in the particular case studied here. Above a certain pitch, the lateral current contributed by the peripheral region saturates, meaning that the short-circuit current of the unit solar cell also saturates. The decrease of the current density J_{sc} observed in Fig. 12 results from dividing a nearly constant total current by an increasing device area. It should be mentioned that, due to different optical models, the photo-generated current density calculated with Sentauros is slightly different from that determined with the geometric

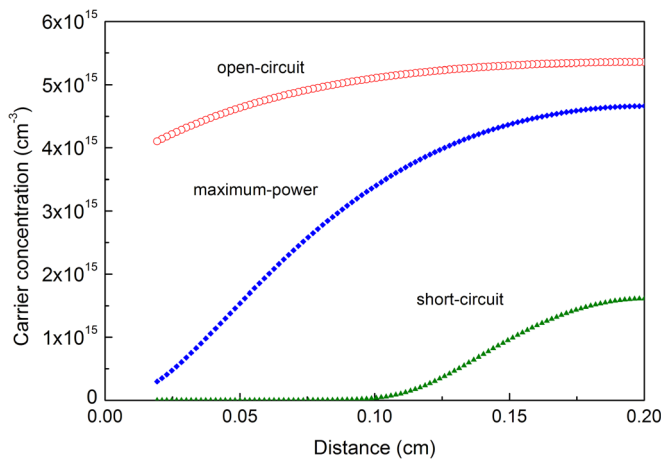


FIG. 13. Minority carrier concentration as a function of the lateral distance for a half-pitch of 0.2 cm and a dopant density $N_A = 10^{15} \text{ cm}^{-3}$ in open-circuit, maximum power and short-circuit conditions. Other parameters are $d = 150 \text{ } \mu\text{m}$, $W = 150 \text{ } \mu\text{m}$ and $J_{0f} = 10^{-13} \text{ A cm}^{-2}$, $J_{0cont} = 10^{-12} \text{ A cm}^{-2}$.

model; in Fig. 12 we have forced the maximum value of J_{sc} calculated with both models to be identical.

Fig. 13 also shows the excess carrier concentration profile in the lateral region corresponding to maximum power conditions, $P = 0.4 \text{ cm}$ and $N_A = 10^{15} \text{ cm}^{-3}$. Comparing it to that corresponding to $N_A = 10^{16} \text{ cm}^{-3}$ in Fig. 8, we can see that the carrier concentration is much higher, with the result of higher recombination losses, leading to a large reduction in J_{mp} to a low value of 24.4 mA cm^{-2} . In addition, resistive losses, mostly in the base region, result in large lateral (109 mV) and crowding (46 mV) voltage drops, equivalent to a very large effective series resistance of $6.2 \text{ } \Omega \text{ cm}^2$, and eventually in a low $V_{mp} = 521 \text{ mV}$ and a very low $FF = 0.49$. The rapid decrease of FF with increasing pitch shown in Fig. 10 for $N_A = 10^{15} \text{ cm}^{-3}$ is therefore attributable to the compounded effect of resistive and recombination losses.

Although not presented here, the simulations were repeated for a lower front surface recombination parameter, $J_{0f} = 10 \text{ fA cm}^{-2}$, representative of advanced technologies. As can be expected, the modeling results indicate that suppressing recombination at the front surface has a beneficial impact on all parameters, particularly on V_{oc} and FF , leading not only to higher efficiencies around 23.5% but also to a broader optimum that is displaced towards higher pitch values.

IV. CONCLUSION

The physical model of Partial Rear Contact solar cells presented in this paper approximates a complex 2D problem by means of a 1D plus 1D analysis of two distinct regions in which the device can be partitioned. The model permits to delve into the physical mechanisms and explain unusual phenomena. Advanced silicon solar cells are usually limited by recombination at the surfaces, hence controlling the diffusion of carriers towards them is the key to their optimization. Indeed, the PRC solar cell design can be viewed as an intelligent implementation of the ideas of diffusivity manipulation to avert surface recombination. The constriction of the flow of carriers towards a small contact area is mathematically and physically equivalent to a reduction of the carrier mobility. This is beneficial to reduce minority carrier recombination at the rear contact, but detrimental to majority carrier flow towards it. A corollary is that PRC solar cells made on n-type silicon wafers can offer advantages compared to the more common p-type devices, thanks to a reversal in majority carrier mobility values.

Computationally, the iterative process required in our model to solve arbitrary device operation conditions is easy to implement and convenient to use. Simplification comes, however, at the expense of generality. In this paper, we have assumed very low bulk recombination and perfect dielectric passivation, leaving as the most significant recombination losses those that occur at the front n^+ electron collector and at the rear p^+ hole collector, or at the rear metal contact. In such conditions, the model is capable of describing the operation of PRC solar cells quite accurately. If significant bulk or surface recombination occurs in the peripheral region the model is no longer applicable in its current simple form. Such cases are, however, of less practical interest for high performance solar cells.

ACKNOWLEDGMENTS

The author is grateful to Di Yan from ANU for the numerical simulations using Sentaurus Device in this paper and to Felix Haase and Jan H. Petermann from ISFH for helpful discussions.

APPENDIX: ANALYTICAL MODEL

It is possible to derive analytical expressions for the open-circuit voltage V_{oc} and the series resistance R_s if a few simplifying assumptions are made. These include low injection conditions, uniform carrier concentration at the front junction, low bulk recombination and a perfectly conducting n^+ front layer.

1. Carrier concentration and open-circuit voltage

The key to derive an analytical solution is to assume that n_f is uniform over the front surface of the solar cell. In addition, we assume here that it is constant as a function of depth in the peripheral region. In low injection, adding recombination at the front surface, at the passivated rear surface, and in the bulk, we can express the recombination current term J_{rec} in Eq. (2) as

$$J_{rec} \approx J_{0f} \frac{n_f}{n_0} + J_{0pass} \frac{n_f}{n_0} + q \frac{n_f W}{\tau_n}, \quad (A1)$$

where $n_0 \approx n_i^2/N_A$ is the equilibrium electron concentration. The net current injected by the peripheral region into the near-contact region I_{net} can be found by subtracting from the total photogeneration occurring in the periphery the sum of all the contributions to recombination in it

$$I_{net} = (J_{ph} - J_{rec})(A_0 - A_{NC}), \quad (A2)$$

where $A_0 = P \times 1$ cm is the aperture area of the unit solar cell and $A_{NC} = 2y_{min} \times 1$ cm is the aperture area of the near-contact region. Next, we determine the electron current at $x = 0$ making use of Eq. (12). To simplify the analysis, let us assume that all the photogeneration J_{ph} happens at the front surface

$$-I_n(0) = I_{net} + A_{NC} J_{ph} - A_{NC} J_{0f} \frac{n_f}{n_0}. \quad (A3)$$

Within the near-contact region let us neglect bulk recombination completely, which permits us to state that the electron current I_n is approximately constant in the vertical direction, that is, $I_n(W) \approx I_n(0)$, so that the boundary condition at the back contact, which gives n_b is

$$-I_n(W) \approx d J_{0cont} \frac{n_b}{n_0} \times 1 \text{ cm}, \quad (A4)$$

where d is the width of the line contact. In low injection, the boundary condition can also be expressed by means of a surface recombination velocity $S_{cont} \approx J_{0cont}/n_0$.

The next step is to integrate Eq. (16), noting that the second term of that expression is zero in open-circuit. In addition, $n(0) = n_f$ and $n(W) = n_b$

$$n_f - n_b = -\frac{I_n}{qD_n} \int_0^W \frac{dx}{A(x)}. \quad (A5)$$

Note that when $I_n < 0$, that is when electrons flow from the front towards the back, $n_f > n_b$. Equation (A5) together with Eqs. (A3) and (A4), results in the following expression for the minority carrier concentration at the front surface

$$n_f = \frac{J_{ph}/q}{\frac{J_{0f}}{qn_0} + \left(\frac{J_{0pass}}{qn_0} + \frac{W}{\tau_n} \right) (1 - f_{NC}) + \left[\frac{qn_0}{f_c J_{0cont}} + \frac{1}{D_n} \int_0^W \frac{A_0}{A(x)} dx \right]^{-1}}. \quad (A6)$$

This expression permits to calculate the open-circuit voltage. It accounts for recombination at the front and rear surfaces as well as in the bulk of the peripheral region, but is, nevertheless, a rough approximation, since it is based on assuming a uniform carrier concentration at the front everywhere in the device, and neglects bulk recombination in the near-contact region. It tends, therefore, to underestimate recombination losses and overestimate V_{oc} .

2. Series resistance

Commencing with the peripheral region, if we completely neglect recombination, the hole current as a function of position is

$$I_p(y) = J_{ph} \left(\frac{P}{2} - y \right) \times 1 \text{ cm}. \quad (A7)$$

The electrostatic potential can be obtained by integrating Eq. (5)

$$\phi(y) = \phi(P/2) - \rho \frac{J_{ph}}{2W} \left(\frac{P}{2} - y \right)^2, \quad (A8)$$

where ρ is the specific resistivity of the material, equal to the inverse of the conductivity, which in low injection is

$$\sigma_p = q\mu_p p \approx q\mu_p N_A. \quad (A9)$$

An equivalent series resistance can be obtained dividing the total voltage drop by the total current

$$R_{s(lat)} = \frac{\rho}{2W} \left(\frac{P}{2} - y_{min} \right) \frac{1}{1 \text{ cm}}. \quad (\text{A10})$$

After replacing $y_{min} = d/2 + W\pi/4$ and multiplying by the area of the half unit cell, the lateral resistance in $\Omega \text{ cm}^2$ is

$$R_{s(lat)}(\Omega \text{ cm}^2) = \rho \frac{P}{8W} \left(P - d - \frac{\pi}{2} W \right). \quad (\text{A11})$$

An alternative derivation based on determining the Joule power loss, rather than the voltage drop, gives a factor 1/12 instead of the factor 1/8 in Eq. (A11). Note that this expression does not include the resistance of the n^+ layer and is not applicable to high injection conditions.

The flow of majority carrier holes towards the local metal contact in the near-contact region comes at the expense of an electrostatic potential difference between the front and back surfaces. To determine it, we integrate the electric field given by Eq. (21), where only the second term is relevant in low injection conditions

$$\phi(0) - \phi(W) = J A_0 \rho \int_0^W \frac{1}{A(x)} dx. \quad (\text{A12})$$

The equivalent series resistance is determined dividing the electrostatic potential difference by the current; we then multiply by the aperture area to express it in $\Omega \text{ cm}^2$

$$R_{s(crowd)} = \rho \int_0^W \frac{A_0}{A(x)} dx. \quad (\text{A13})$$

For the case of linear contacts separated by a large pitch, the integral can be performed analytically for the function given by Eq. (15); the equivalent “crowding” resistance is

$$R_{s(crowd)} = \rho \frac{P}{\pi} \ln \left(1 + \frac{W}{d/\pi} \right). \quad (\text{A14})$$

When all recombination is neglected except at the contact, the carrier concentration at the front is, for large pitch values

$$n_f = n_b + \frac{J_{ph}}{qD_n} \frac{P}{\pi} \ln \left(1 + \frac{W}{d/\pi} \right). \quad (\text{A15})$$

The formal similarity between the expressions for the carrier concentration when recombination is neglected (A15) and the crowding resistance (A14) was already noted by Fischer. The sum of Eqs. (A11) and (A14) gives the total series resistance, apart from possible metal-semiconductor contact resistance and additional components due to the front diffusion and metal grid.

- ¹D. Reinwand, J. Specht, D. Stuwe, S. Seitz, J. Nekarda, D. Biro, R. Preu, and R. Trassl, in *35th IEEE Photovoltaic Specialists Conference*, Honolulu, 2010 (IEEE), 003582.
- ²Y. Gassenbauer, K. Ramspeck, B. Bethmann, K. Dressler, J. D. Moschner, M. Fiedler, E. Brouwer, R. Drössler, N. Lenck, F. Heyer, M. Feldhaus, A. Seidl, M. Muller, and A. Metz, *IEEE J. Photovoltaics* **3**, 125 (2013).
- ³S. Baoming, S. Jian, Y. Shengzhao, Z. Chun, F. Zhiqiang, and H. Qiang, in *38th IEEE Photovoltaic Specialists Conference*, Austin, TX, 2012, 001125.
- ⁴A. G. Aberle, G. Heiser, and M. A. Green, *J. Appl. Phys.* **75**, 5391 (1994).
- ⁵H. Plagwitz and R. Brendel, *Prog. Photovoltaics* **14**, 1 (2006).
- ⁶A. Cuevas, *IEEE J. Photovoltaics* **2**, 485 (2012).
- ⁷B. Fisher, Ph.D. dissertation, University of Konstanz, 2003.
- ⁸P. Saint-Cast, M. Rudiger, A. Wolf, M. Hofmann, J. Rentsch, and R. Preu, *J. Appl. Phys.* **108**, 013705 (2010).
- ⁹A. Kimmerle, M. Rüdiger, A. Wolf, M. Hermle, and D. Biro, *Energy Procedia* **27**, 219 (2012).
- ¹⁰A. Wolf, D. Biro, J. Nekarda, S. Stumpp, A. Kimmerle, S. Mack, and R. Preu, *J. Appl. Phys.* **108**, 124510 (2010).
- ¹¹Sentaurus Process User Guide, Version E-2010-12, Synopsys, Inc., Mountain View, CA (2010).
- ¹²P. A. Basore and K. Cabanas-Holmen, *IEEE J. Photovoltaics* **1**, 72 (2011).
- ¹³R. Brendel, *Prog. Photovoltaics* **20**, 31 (2012).
- ¹⁴A. Fell, *IEEE Trans. Electron Devices* **60**, 733 (2013).
- ¹⁵A. Cuevas and J. H. Petermann, *IEEE J. Photovoltaics* **3**, 587 (2013).
- ¹⁶J. A. del Alamo and R. M. Swanson, *IEEE Trans. Electron Devices* **31**, 1878 (1984).
- ¹⁷P. Würfel, *Physics of Solar Cells: From Basic Principles to Advanced Concepts* (Wiley, 2009).
- ¹⁸P. A. Basore, *IEEE Trans. Electron Devices* **37**, 337 (1990).
- ¹⁹S. C. Baker-Finch and K. R. McIntosh, *Prog. Photovoltaics* **20**, 51 (2012).
- ²⁰M. A. Green, *Sol. Energy Mater. Sol. Cells* **92**, 1305 (2008).
- ²¹M. J. Kerr and A. Cuevas, *J. Appl. Phys.* **91**, 2473 (2002).
- ²²A. Cuevas and R. A. Sinton, in *Proceedings 23rd European Photovoltaic Solar Energy Conference*, Valencia, Spain, 2008 (WIP-Renewable Energies), p. 315.
- ²³A. Cuevas, *Energy Procedia* **8**, 94 (2011).
- ²⁴A. Cuevas, D. Yan, F. Haasse, J. Petermann, and R. Brendel, “A comparison of models to optimize Partial Rear Contact solar cells,” *Energy Procedia* (to be published).